CHAPTER 6

THE MORPHOTROPIC PHASE BOUNDARY AND DIELECTRIC PROPERTIES OF xPb($Zr_{1/2}Ti_{1/2}$)O_3 − (1-x)Pb($Ni_{1/3}Nb_{2/3}$)O_3 PEROVSKITE SOLID SOLUTION

Overview -The solid solution between the normal ferroelectric Pb($Zr_{1/2}Ti_{1/2}$)O_3 (PZT) and relaxor ferroelectric Pb($Ni_{1/3}Nb_{2/3}$)O_3 (PNN) was synthesized by the columbite method. The phase structure and dielectric properties of xPZT−*(1-x)*PNN where $x = 0.4 - 0.9$ and the Zr/Ti composition was fixed close to the MPB were investigated. With these data, the ferroelectric phase diagram between PZT and PNN has been established. The relaxor ferroelectric nature of PNN gradually transformed towards a normal ferroelectric state towards the composition *0.7*PZT-*0.3*PNN, in which the permittivity was characterized by a sharp peak and the disappearance of dispersive behavior. XRD analysis demonstrated the coexistence of both the rhombohedral and tetragonal phases at the composition *0.8*PZT-*0.2*PNN; a new morphotropic phase boundary within this system. Examination of the dielectric spectra indicates that PZT-PNN exhibits an extremely high relative permittivity near the MPB composition. The permittivity shows a shoulder at the rhombohedral to tetragonal phase transition temperature, T_{RT} = 195°C, and then a maximum permittivity (36,000 at 10 kHz) at the transition temperature T_{max} = 277°C at the MPB composition.

ลิขสิทธิ์มหาวิทยาลัยเชียงใหม่
Copyright © by Chiang Mai University
All rights reserved

6.1 Introduction

The relaxor ferroelectric lead nickel niobate [$Pb(Ni_{1/3}Nb_{2/3})O_3$, PNN] has been studied by numerous researchers since its discovery by Smolenskii and Agranovskaya in 1958.[4] At room temperature, single crystal PNN has the cubic prototype symmetry *Pm3m* with a lattice parameter (*a*) = 4.03Å.[40] Nanometer-level chemical heterogeneity in the form of short range ordering of Ni^{2+} and Nb^{5+} on the B-site was proposed to account for the diffuse phase transition.[10,40] The complex perovskite shows a broad maximum of the dielectric permittivity near -120°C with relative permittivity near 4,000 at 1 kHz.[47]

In the last decade, normal ferroelectric lead zirconate titanate [$Pb(Zr_{1-x}Ti_x)O_3$, PZT] has become one of the most important commercially produced piezoelectric materials.[6] Excellent piezoelectric properties have been observed in compositions close to the morphotropic phase boundary (MPB Zr:Ti ~52:48).[2] Recently, many piezoelectric ceramic materials have been developed from binary systems containing a combination of relaxor and normal ferroelectric materials[60] which yield high dielectric permittivities (e.g. PMN–PT[54], PZN–PT[25], PMN–PZT[61]), excellent piezoelectric coefficients (e.g. PZN–PT[25,62], PZN–PZT[39], PSN–PT[59,63]), and high pyroelectric coefficients (e.g. PNN-PT-PZ[43]).

Fan and Kim[24] investigated the solid solution within the PZN-PZT binary system in which the Zr/Ti composition was close to the MPB. This study indicated the composition *0.5*PZN–*0.5*PZT showed the optimal piezoelectric properties. Moreover, these properties could be improved by thermal treatments.

In 1974 Luff *et al.*[43] investigated solid solution in the PNN–PZ–PT ternary system and observed excellent piezoelectric properties at the composition *0.5*PNN–

ลิขสิทธิ์มหาวิทยาลัยเชียงใหม่
Copyright © by Chiang Mai University
All rights reserved

*0.35*PT–*0.15*PZ. There have been numerous papers published dealing with piezo-electric and processing issues within this compositional family.[42,43,45,64] These compositions have found wide applications and are now commercially available. However, there is limited information in the literature on the PNN–PZT system with Zr/Ti close to the MPB. Detailed reaction kinetics using conventional solid state processing of $Pb(Ni_{1/3}Nb_{2/3})O_3$–$Pb(Zr_{0.48}Ti_{0.52})O_3$ was recently investigated by Babushkin.[64] A sequence of pyrochlore phases was detected at different temperatures, but there is no information pertaining to the dielectric and ferroelectric properties. Since PNN is a relaxor ferroelectrics with a broad dielectric peak near $T_c \sim$ -120°C and PZT (Zr/Ti = 50/50) is a normal ferroelectric with a sharp maximum permittivity at $T_c \sim 390$°C, the curie temperature in PNN-PZT system can be engineered over a wide range of temperature by controlling the amount of PZT in the system. The aim of this work was to investigate the quasi-binary solid solution *x*PZT (Zr/Ti = 50/50) – *(1-x)*PNN, with $x = 0.4 - 0.9$. Fig. 6.1 schematically shows the pseudo-ternary composition range which was studied in this work compared with other studies.[43,45,46,55,64,65] Although pure PNN-PZ-PT ternary ceramics can be fabricated by conventional methods[43], the B-site precursor method is a better method for enhancing the dielectric properties and ferroelectric properties.

ลิขสิทธิ์มหาวิทยาลัยเชียงใหม่
Copyright © by Chiang Mai University
All rights reserved

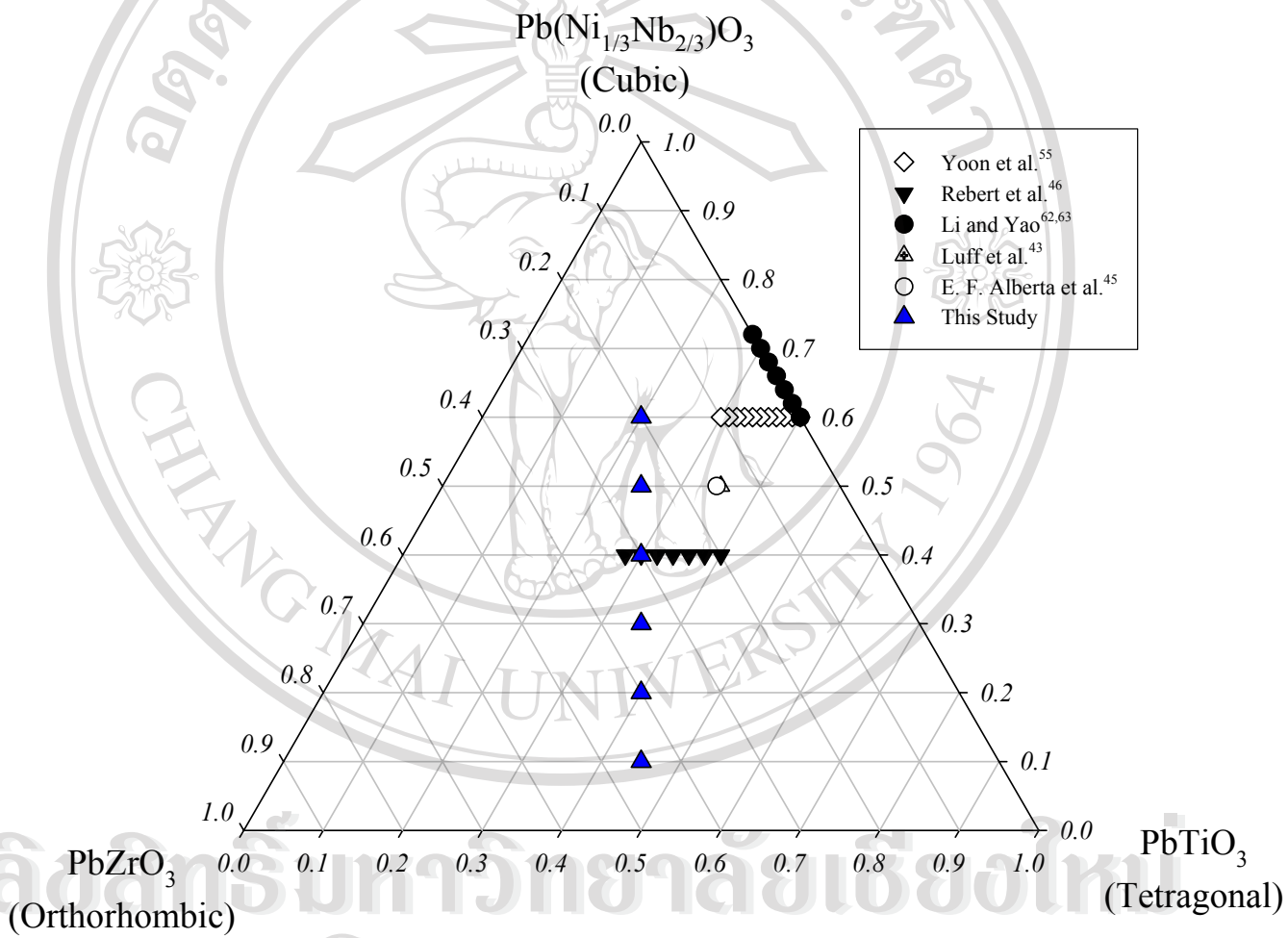

Figure 6.1 Compositions studied in the $Pb(Ni_{1/3}Nb_{2/3})O_3$-$PbZrO_3$-$PbTiO_3$ ternary system.

ลิขสิทธิ์มหาวิทยาลัยเชียงใหม่
Copyright © by Chiang Mai University
All rights reserved

This process involves pre-reacting the B-site cations to form the columbite phase $NiNb_2O_6$ and the wolframite phase $ZrTiO_4$. With this method it is possible to obtain a homogeneous perovskite solid solution without the other constituent perovskite phases such as PZ, PT, PZT, PNN and the formation of the parasitic pyrochlore phases is prevented. Finally, the nature of the relaxor-normal ferroelectric phase transition was studied through a combination of dielectric measurements and x-ray diffraction.

6.2 Experimental procedure

The powders of *x*PZT – *(1-x)*PNN were synthesized using the columbite precursor method. Reagent-grade oxide powders of PbO, ZrO_2, TiO_2, NiO and Nb_2O_5, were used as raw materials. The columbite structure ($ZnNb_2O_6$) and wolframite structure ($ZrTiO_4$) were synthesized first. Stoichiometric amounts of the precursors (NiO, Nb_2O_5) and (ZrO_2, TiO_2) were mixed and milled in isopropyl alcohol for 6 hours using a vibratory mill. The mixture was dried at 60^{o}C for 12 hours. The precursors $NiNb_2O_6$ and $ZrTiO_4$ were calcined at 975^{o}C and 1400^{o}C, respectively, for 4 hours in a closed alumina crucible. The calcined $NiNb_2O_6$ and $ZrTiO_4$ powders were mixed with PbO in a stoichiometric ratio to form the composition *x*PZT – *(1-x)*PNN, where $x = 0.4 - 0.9$ (shown in Fig 6.1). In all composi-tions, 2 mol % excess PbO was added to compensate for lead volatilization during calcination and sintering. After re-milling and drying, the mixtures were calcined at 950^{o}C for 4 hours in a double alumina crucible configuration with a heating rate of 10 ^{o}C/min.

ลิขสิทธิ์มหาวิทยาลัยเชียงใหม่
Copyright © by Chiang Mai University
All rights reserved

The calcined powders were milled for 3 hours for reduced particle size. After grinding and sieving, the calcined powder was mixed with 5 wt% poly (vinyl alcohol) binder and uniaxially pressed into a pellet. Binder burnout occurred by slowly heating to 500°C and holding for 2 hours. Sintering occurred between 1100 - 1250°C with a dwell time of 4 hours. To mitigate the effects of lead loss during sintering, the pellets were sintered in a closed alumina crucible containing $PbZrO_3$ powder. The perovskite phase was examined by x-ray diffraction (XRD). Data collection was performed in the 2θ range of 20° – 70° using step scanning with a step size of 0.02° and counting time of 2s/step.

After surface grinding, the samples were electroded using sputtered gold and air-dried silver paint was applied. The relative permittivity (ε_r) and dissipation factor ($tan\delta$) were measured using an automated measurement system. This system consisted of an LCR meter (HP-4284A, Hewlett-Packard Inc.) in connection with a Delta Design 9023 temperature chamber and a sample holder (Norwegian Electroceramics) capable of high temperature measurement. The capacitance and dissipation factors of sample were measured at 100 Hz, 1 kHz, 10 kHz and 100 kHz and temperature varied between 25 – 450°C. A heating rate of 3°C/minute was used during measurements.

Samples were prepared for optical analysis by polishing with SiC paper through 1200-grit. Raman spectra were measured using a Renishaw inVia Reflex Raman microscope and 488 nm radiation from a laser excitation source. The laser had an output power of 25 mW and a focused spot size of 200-300 μm through a 5x microscope objective. Raman spectra were measured using a static acquisition centered at 520 cm^{-1} and 15 accumulations with 2 second exposure times.

ลิขสิทธิ์มหาวิทยาลัยเชียงใหม่
Copyright © by Chiang Mai University
All rights reserved

6.3 Results and discussion

6.3.1. Crystal structure and phase transition studies

Perovskite phase formation, crystal structure and lattice parameter was determined by XRD at room temperature as a function of *x*. Fig. 6.2 shows XRD patterns of ceramics in the *x*PZT – *(1-x)*PNN system with a well crystallized perovskite structure for all compositions. The pyrochlore phase was not observed in this system at all. The crystal symmetry for pure PNN at room temperature is cubic *Pm3m* with a lattice parameter a = 4.031 Å. Below T_{max} = -120°C, the symmetry changes to rhombohedral. The crystal structure of $Pb(Zr_{1/2}Ti_{1/2})O_3$ at room temperature is tetragonal. Therefore, with increasing *x* the crystal symmetry should change due to the effects of the increased PZT fraction and the increase in T_C. Fig. 6.3 shows XRD peak profiles of the (200) and (220) peaks at *x = 0.4, 0.5,* and *0.6*. The XRD data shows no splitting of (200). At the *x* = 0.4 composition, only a single (220) peak is observed, indicating that the major phase in this composition has cubic symmetry. However, splitting was clearly observed for the (220) peak in compositions *x = 0.5* and *0.6*, indicating that the crystal transformed into rhombohedral symmetry (pseudo-cubic). With a further increase in PZT content to *x > 0.6*, the (111) and (200) diffraction peaks begin to split as shown in Fig 6.4. Splitting of the (200) peak becomes more pronounced as *x* approaches *0.9* indicating a stabilization of the tetragonal phase at high PZT concentrations.

ลิขสิทธิ์มหาวิทยาลัยเชียงใหม่
Copyright © by Chiang Mai University
All rights reserved

At the *x = 0.8* composition, the unambiguous splitting of (111) peak indicates the co-existence of the rhombohedral and tetragonal phase. Thus there is a transformation from the rhombohedral phase to the tetragonal phase across the compositional

range *x = 0.7-0.9*. The *x = 0.7* composition is within the rhombohedral-rich side of the MPB and the composition *x = 0.9* is on the tetragonal-rich side of the MPB. It is important to note that recent results have uncovered the existence of a low-symmetry (monoclinic) phase within the MPB region of PZT[66], PMN-PT[67] and the orthorhombic phase of PZN-PT.[68] Given the similarities of PNN-PZT to the PMN-PT system, it is possible that a low symmetry monoclinic or orthorhombic phase may be stabilized within the MPB regions of *x*PZT – *(1-x)*PNN; *x = 0.7-0.9*.

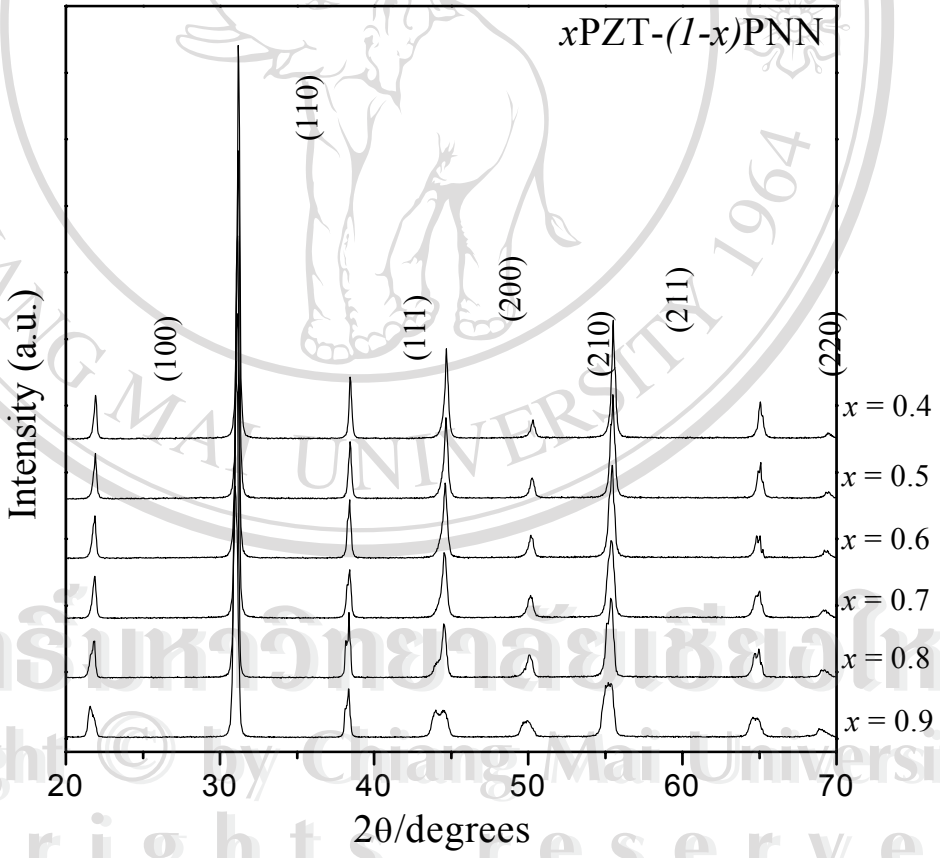

Figure 6.2 X-ray diffraction patterns at room temperature for *x*PZT – *(1-x)*PNN ceramics.

ลิขสิทธิ์มหาวิทยาลัยเชียงใหม่
Copyright © by Chiang Mai University
All rights reserved

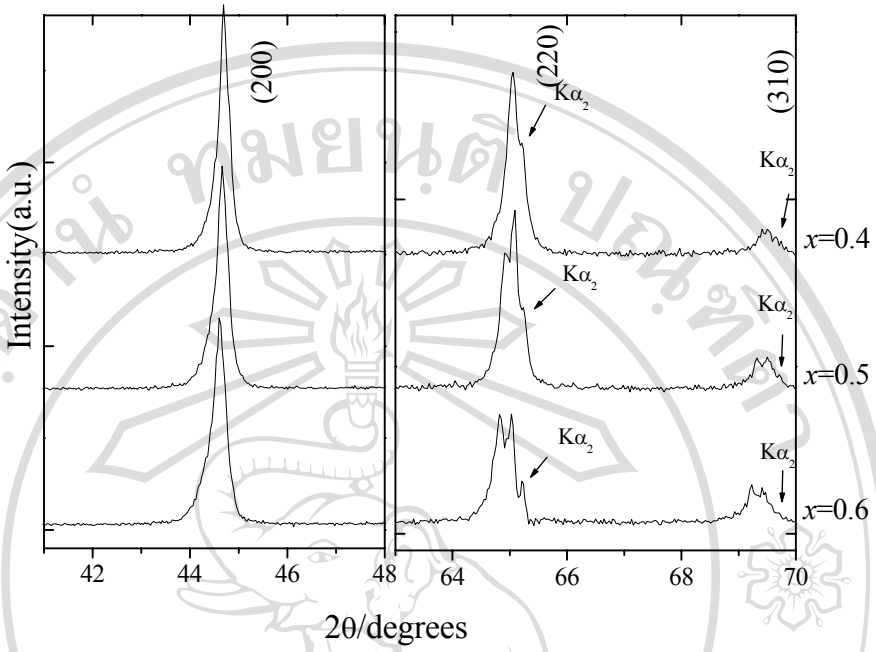

Figure 6.3 X-ray pattern of the (200) and (220) peak of *x*PZT – *(1-x)*PNN, *x = 0.4-0.6* ceramics.

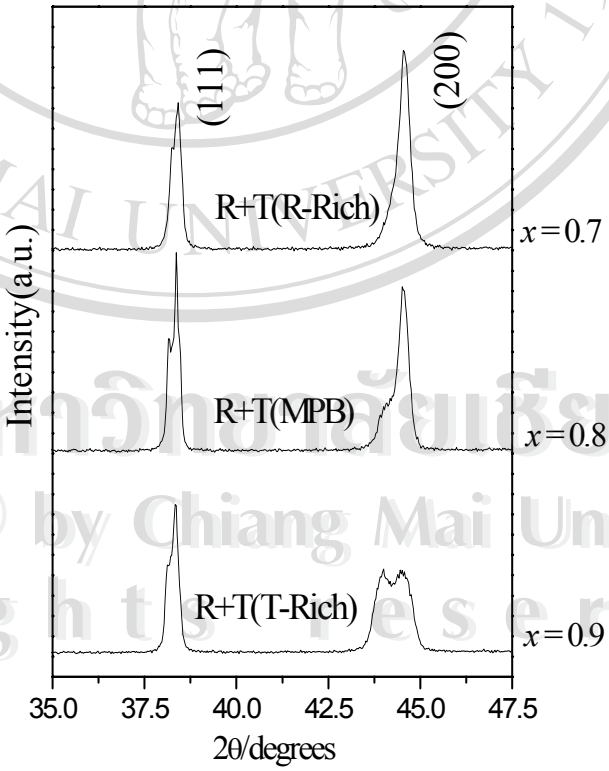

Figure 6.4 X-ray pattern of the (111) and (200) peak of *x*PZT – *(1-x)*PNN, *x = 0.6-0.9* ceramics.

ลิขสิทธิ์มหาวิทยาลัยเชียงใหม่
Copyright © by Chiang Mai University
All rights reserved

6.3.2 Dielectric properties

The characteristic temperature and frequency dependence of the relative permittivity for *x*PZT–(*1-x*)PNN, *x = 0.4 - 0.9* is shown in Fig. 6.5 A clear transition in T_{max} (defined as the temperature at which ε_r is maximum at 10 kHz) is observed with T_{max} increasing with *x*. At compositions *x = 0.4*, *0.5* and *0.6*, the sample displays a pronounced relaxor ferroelectric behavior, characterized by diffuse permittivity peaks and a shift of the maximum permittivity to higher temperatures with increasing frequency. An increase in the magnitude of the maximum permittivity is also observed over this region. The nature of the homogeneously polarized states is believed to be controlled by the concentration of PZT.

A smooth transition from relaxor to normal ferroelectric behavior is observed with increasing mole percent of PZT from *x = 0.7* to *0.9*. This transition is characterized by the enhancement of the first-order nature of the phase transformation and the diminishment of the relaxor behavior (i.e. the permittivity dispersion) over the broad temperature range in the vicinity of T_{max}. From these data, the relaxor–normal transformation is very clearly observed with increased PZT concentration above *x = 0.7*. Furthermore, the relative permittivity and T_{max} increased with increased mole percent of PZT considerably up to a maximum permittivity at *x = 0.8*. The sharp permittivity peak exhibits a maximum value of 36,000 at 10 kHz for this composition. Fig. 6.6 shows a comparison of the permittivity as a function of temperature for the compositions *x = 0.5*, *0.7*, and *0.8* taken over the measurement frequencies of 100 Hz - 100 kHz.

For *x = 0.5*, T_{max} increases from 125.6°C at 100 Hz to 130.8°C at 100 kHz ($\Delta T = 5.2^{o}C$). The relative permittivity at room temperature was 2,830 at 100 Hz and

ลิขสิทธิ์มหาวิทยาลัยเชียงใหม่
Copyright © by Chiang Mai University
All rights reserved

increased to 24,200 at 1 kHz at T_{max}, and the maximum value of the relative permittivity decreased with increasing frequency. The dielectric dispersion below T_{max} indicates typical relaxor ferroelectric behavior arising from the responses of polar micro-domains within the spectrum of the relaxation time. For *x = 0.7* and *0.8* compositions, it is evident that two phase transitions are observed. Over the temperature range 190 to 200°C, a rhombohedral to tetragonal phase transition is observed for both compositions (indicated in the figure by $T_{Rho\text{-}Tetra}$).

Another transition between the ferroelectric tetragonal to paraelectric cubic phase occurs in the temperature ranges 225°C and 277°C for *x = 0.7* and *x = 0.8*, respectively. Although the transition from ferroelectric rhombohedral to tetragonal phase is obscured in the composition *x = 0.7* it is more clearly evident in the composition *x = 0.8*. Similar phenomena have been observed in single crystal PZN–PT[62], PIN–PT[69], and PMN–PT[54].

In addition, the transformation from the relaxor ferroelectric state to the normal ferroelectric state can be observed in the composition *x = 0.7-0.9* as shown in Figs. 6.5, 6.6(b), 6.6(c). The permittivity sharply increased near the temperature indicated as $T_{start\ NR}{}^{*}$ in Figs. 6.6(b) and 6.6(c). Relaxor behavior was observed at temperatures above $T_{finish\ NR}{}^{**}$.

ลิขสิทธิ์มหาวิทยาลัยเชียงใหม่
Copyright © by Chiang Mai University
All rights reserved

---

* The subscript "start NR" denotes the initial transition from a normal ferroelectric state to a pure relaxor ferroelectric state.

** The subscript "finish NR" denotes the completion of the transformation.

For $x = 0.7$ at temperatures below 212°C, the relative permittivity did not show any significant dispersion until 218°C. Above this temperature, the relative permittivity shows a strong frequency dependence. This indicates that at 212°C, 0.7PZT–0.3PNN started to transform from a normal ferroelectric state to a relaxor ferroelectric state; finishing the transformation at 218°C. The differential between $T_{start\ NR}$ and $T_{finish\ NR}$ was approximately 6°C, 5°C and 4°C for x = 0.7, 0.8, 0.9 respectively. This behavior can be explained by decreasing relaxor stability with increasing x. At the composition $x = 0.9$, a broad permittivity was observed with a slight frequency dispersion close to T_{max}. A first-order transition response was observed at temperatures slightly below T_{max}. This phenomenon indicates that the polar moments are static, since the polar moments are relative large. The crystal structure and dielectric properties for all compositions are listed in Table 6.1

ลิขสิทธิ์มหาวิทยาลัยเชียงใหม่
Copyright © by Chiang Mai University
All rights reserved

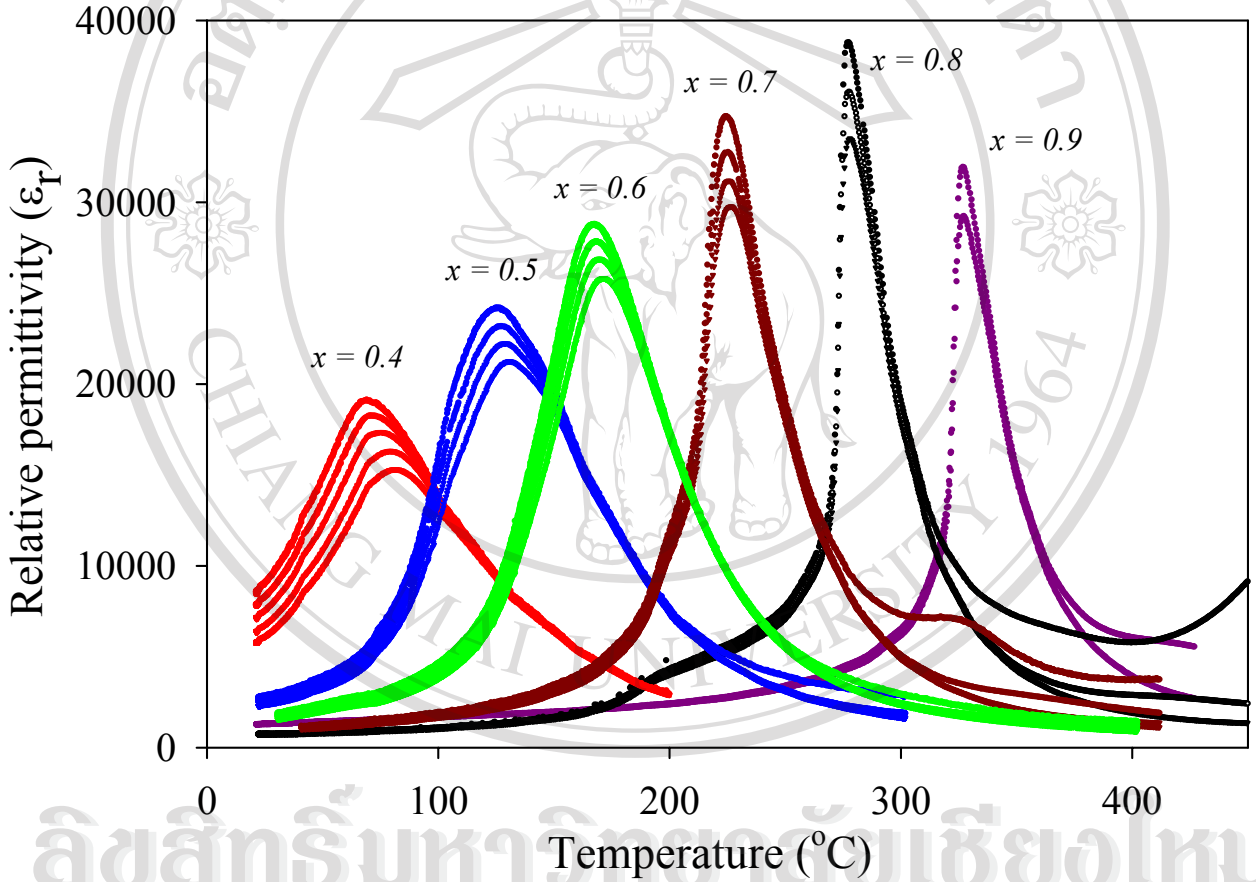

Figure 6.5 Temperature dependence of relative permittivity ε_r for *x*PZT – *(1-x)*PNN, *x = 0.4-0.9* ceramic.

ลิขสิทธิ์มหาวิทยาลัยเชียงใหม่
Copyright © by Chiang Mai University
All rights reserved

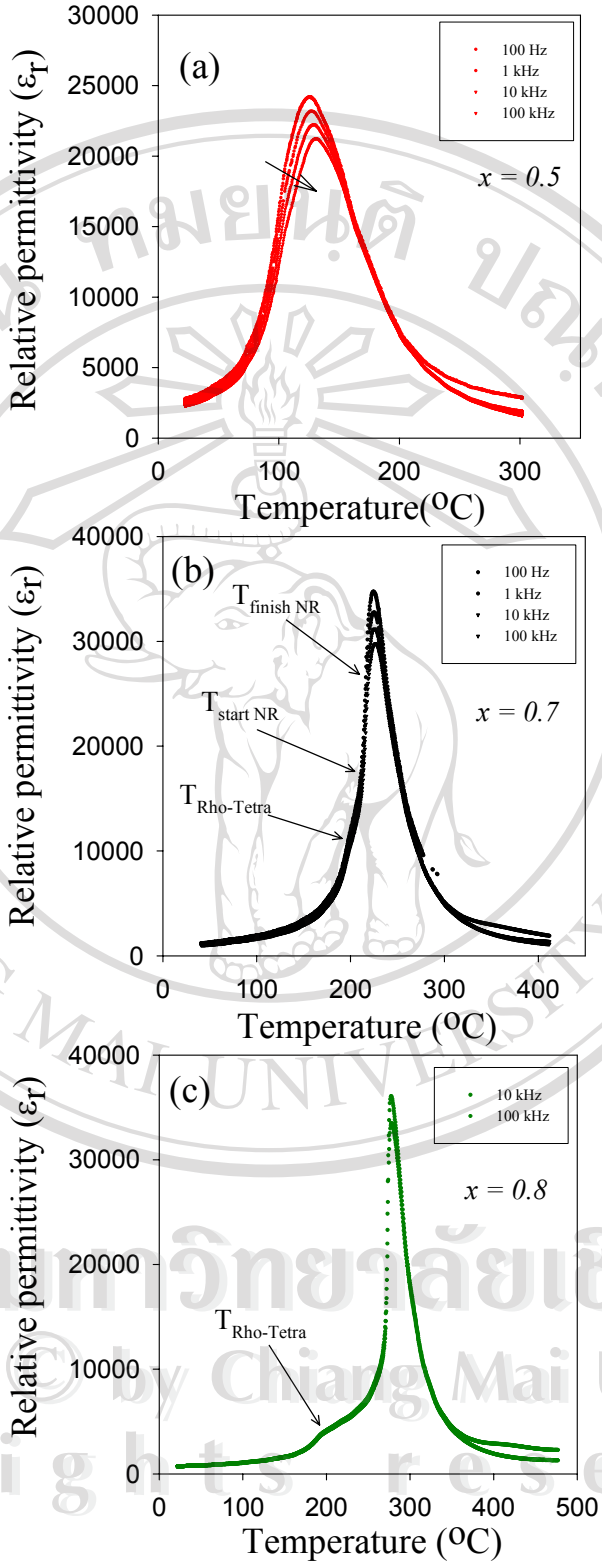

Figure 6.6 Temperature dependence of relative permittivity ε_r for *x*PZT – *(1-x)*PNN, a: $x = 0.5$, b: $x = 0.7$ and c: $x = 0.8$ ceramics is shown.

ลิขสิทธิ์มหาวิทยาลัยเชียงใหม่
Copyright © by Chiang Mai University
All rights reserved

Table 6.1 Dielectric properties of *x* PZT– (*1-x*) PNN ceramics.

Composition *x*	Crystal structure	T_m(°C) at 10 kHz	Relative permittivity at 25°C	Relative permittivity at T_{max}	tan δ at 25°C	tan δ at T_m	δ_γ
x = 0.4	C	75.4	7500	17500	0.062	0.036	29.5
x = 0.5	R	128.9	2500	22000	0.042	0.024	24.4
x = 0.6	R	169.7	1600	27000	0.042	0.018	22.4
x = 0.7	R-rich	225.5	1060	31200	0.029	0.025	14.0
x = 0.8	R+T	277.4	835	36000	0.011	0.047	10.2
x = 0.9	T-rich	326.7	950	32000	0.005	0.182	8.6

C = cubic, R = rhombohedral, T = tetragonal

ลิขสิทธิ์มหาวิทยาลัยเชียงใหม่
Copyright © by Chiang Mai University
All rights reserved

The maximum permittivity $\varepsilon_{r,max}$ and T_{max} as a function of the mole fraction of PZT (x) are represented in Fig. 6.7 There is a good linear relationship between T_{max} and x, indicating that this system is a well behaved complete solid solution. The T_{max} of the constituent compounds PNN and PZT are –120°C and 390°C, respectively, which can be used to calculate an empirical estimate of T_{max} via the equation:

$$T_{max} = x(390^{o}C) + (1-x)(-120^{o}C) \tag{6.1}$$

The variation of the measured T_{max}, the calculated T_{max}, and the measured $\varepsilon_{r,max}$ as a function of composition x is shown in Fig. 6.7 The highest $\varepsilon_{r,max}$ of 36,000 at 277°C at 10 kHz was observed for the composition at the MPB *0.8*PZT-*0.2*PNN. It is evident from the data that Eq. (6.1) gives a reasonable approximation of the transition temperature T_{max}. This result suggests that the transition temperature of *x*PZT–(*1*-*x*)PNN system can be varied over a wide range from -120 to 390°C by controlling the amount of PZT in the system.

It is well known that the permittivity of a first-order normal ferroelectric can be described by the Curie-Weiss law and a second order relaxor ferroelectric can be described by a simple quadratic law. This arises from the fact that the total number of relaxors contributing to the permittivity response in the vicinity of the permittivity peak is temperature dependent, and the temperature distribution of this number is given by a Gaussian function about a mean value T_o with a standard deviation δ. The relative permittivity can be derived via using the equation (5.2)

ลิขสิทธิ์มหาวิทยาลัยเชียงใหม่
Copyright © by Chiang Mai University
All rights reserved

The values γ and δ_γ are both material constants depending on the composition and structure of the material. The δ_γ value can be determined from the intercept of $\varepsilon'_m / \varepsilon'$ versus $(T\text{-}T_m)^2$, which should be linear. The δ_γ values of compositions in the *x*PZT–(*1-x*)PNN system are represented in Fig 6.8.

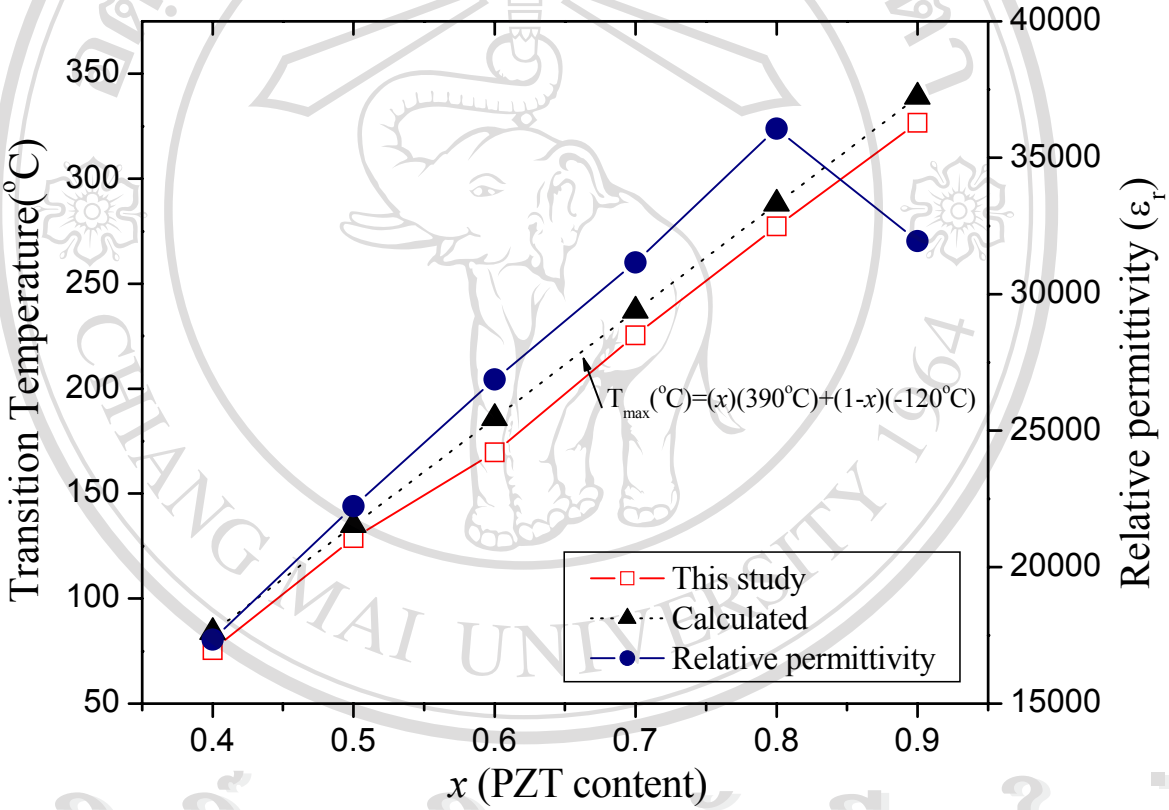

Figure 6.7 T_{max}, Calculated T_{max} and Maximum ε_r as a function of composition *x* at 10 kHz.

ลิขสิทธิ์มหาวิทยาลัยเชียงใหม่
Copyright © by Chiang Mai University
All rights reserved

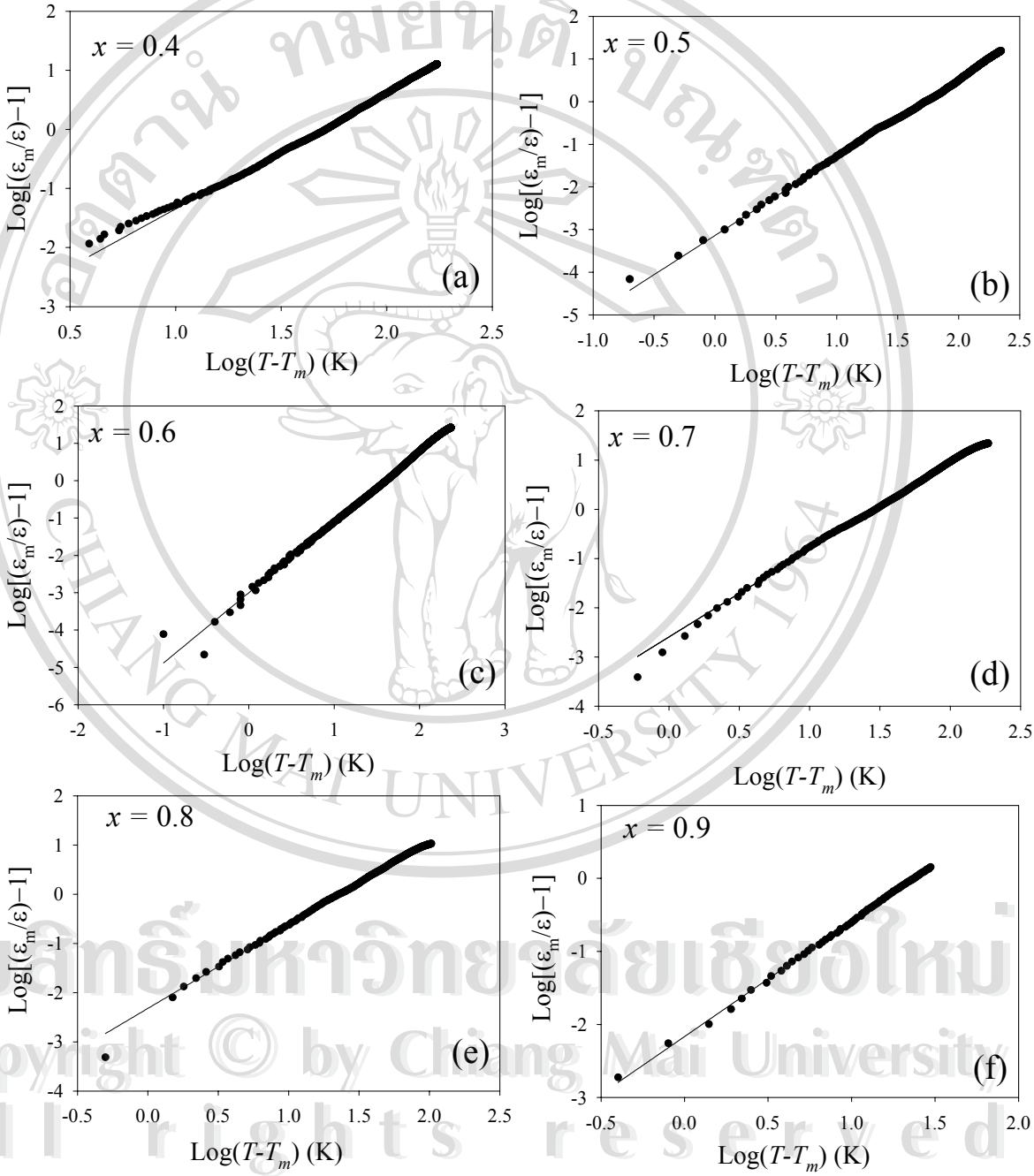

Figure 6.8 Dependence of Log [(ε_m/ ε)-1] with Log(T-T_{max}) for *x*PZT – *(1-x)*PNN, *x = 0.4-0.9* ceramics.

ลิขสิทธิ์มหาวิทยาลัยเชียงใหม่
Copyright © by Chiang Mai University
All rights reserved

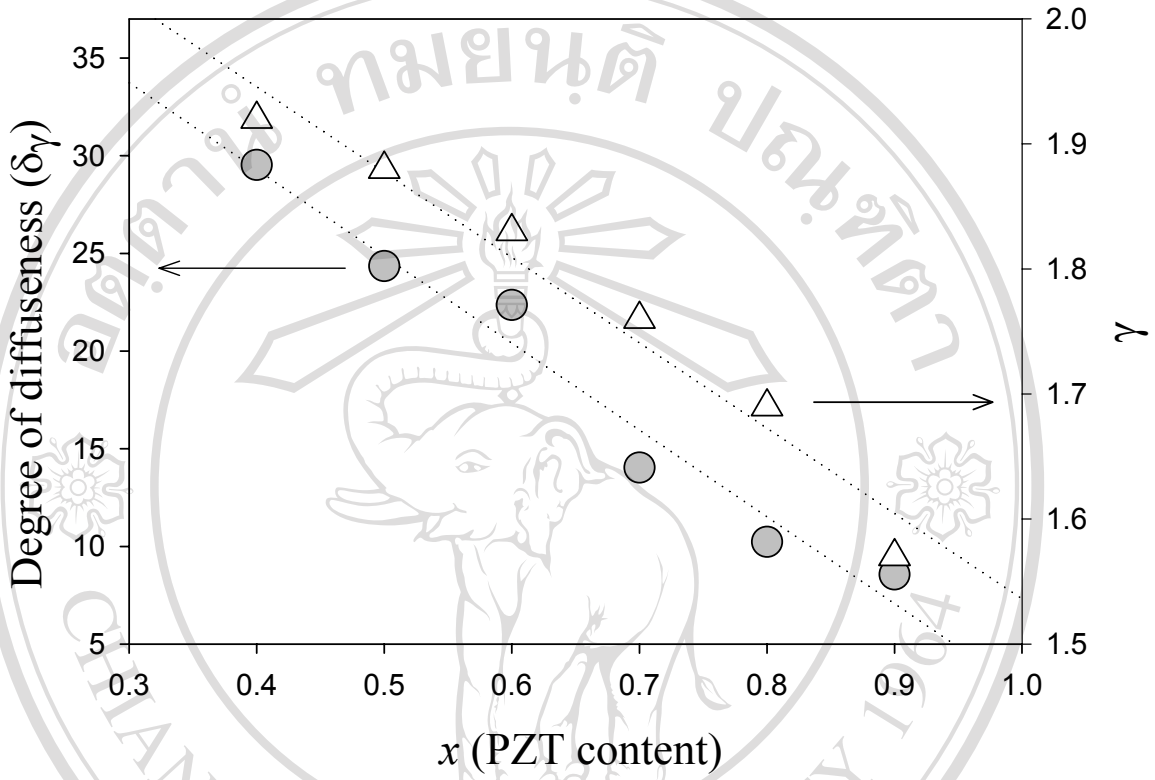

Figure 6.9 Dependence of γ and degree of diffuseness (δ_γ) for *x*PZT – *(1-x)*PNN, *x = 0.4-0.9* ceramics.

Both the diffuseness parameter δ_γ and γ decreased with an increase in the mole fraction of PZT. As illustrated in Fig. 6.9, a near linear relationship was observed over the wide compositional range which is consistent with a perfect solid solution. The diffuseness of the phase transition in the *x = 0.4* composition can be attributed to the relaxor nature of PNN. As the PZT content increased, the relaxor characteristic of *x*PZT – (*1-x*)PNN was observed to decrease. This is because the substitution of $(Zr_{1/2}Ti_{1/2})^{4+}$ for the B-site complex ions $(Ni_{1/3}Nb_{2/3})^{4+}$ increases the size of the local polar domains by strengthening the off-center displacement and enhancing the

ลิขสิทธิ์มหาวิทยาลัยเชียงใหม่
Copyright © by Chiang Mai University
All rights reserved

interactions between micro-polar domains. As observed in PMN-PT crystals[70], this leads to the formation of macro-polar domains which break the symmetry of the pseudo-cubic state.

6.3.3 Phase diagram of $Pb(Zr_{1/2}Ti_{1/2})O_3$–$Pb(Ni_{1/3}Nb_{2/3})O_3$

Based on the results of x-ray diffraction, dielectric spectroscopy, and Raman spectroscopy, the phase diagram for the *x*PZT–(*1-x*)PNN binary system have been established, shown in Fig. 6.10 The transition temperature increases approximately linearly with *x*, from T_{max} = 75°C for *x = 0.4* to 340°C for *x = 0.9*. The phase diagram consists of four distinct crystallographic phases in this system; high temperature paraelectric cubic (*Pm3m*), pseudo-cubic relaxor, rhombohedral relaxor (*R3m*), and normal ferroelectric tetragonal (*P4mm*). At low concentrations of PZT $x \leq 0.4$ the symmetry of can be defined as pseudo-cubic. The pseudo-cubic symmetry transforms into rhombohedral at the composition near *x = 0.5*. The ferroelectric rhomohedral and tetragonal phases are separated by a morphotropic phase boundary (MPB) region which is located near the composition *x = 0.8* below 277°C. Within this region, both the rhomohedral and tetragonal phases coexist.

ลิขสิทธิ์มหาวิทยาลัยเชียงใหม่
Copyright © by Chiang Mai University
All rights reserved

6.4. Conclusions

In this work the ferroelectric properties of the solid solution between relaxor ferroelectric PNN and normal ferroelectric PZT(50/50) have been investigated. The crystal structure data obtained from XRD indicates that the solid solution *x* PZT-(*1-x*)PNN, where *x = 0.4-0.9*, successively transforms from pseudo-cubic to rhombohedral to tetragonal symmetry with an increase in PZT concentration. The

new MPB in this binary system is located near $x = 0.8$, separating the rhombohedral and tetragonal phases. At the MPB composition, the permittivity exhibited a shoulder at T_{RT} = 195 °C indicating a rhombohedral to tetragonal phase transformation with a maximum permittivity of 36,000 at 10 kHz at T_{max} = 277 °C. Moreover a transition from relaxor to normal ferroelectric behavior is clearly observed above a PZT concentration $x = 0.7$. Furthermore, this transition between relaxor to normal ferroelectricity was typified by a quasi-linear relationship between the diffuseness parameter δ_γ and PZT mole fraction x.

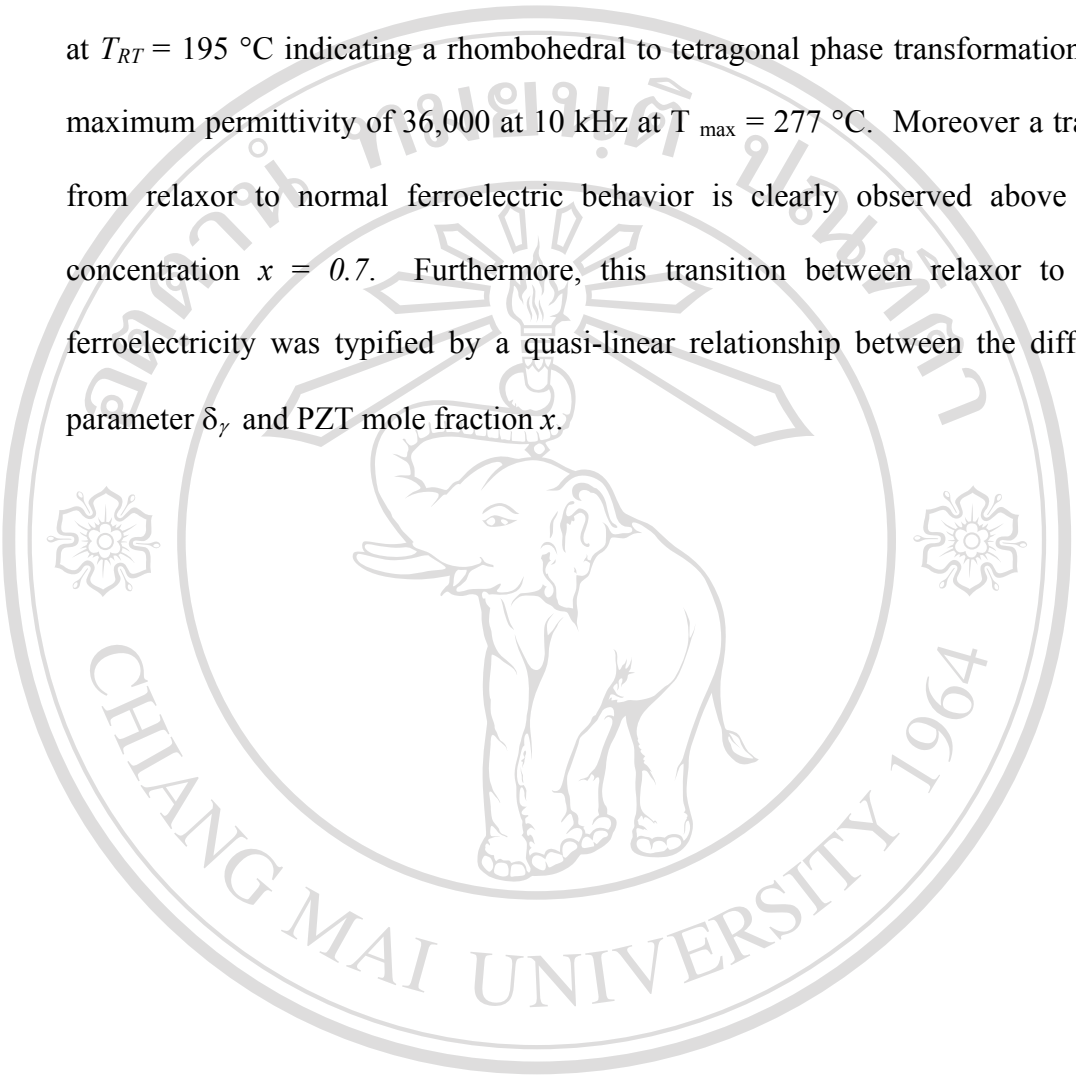

ลิขสิทธิ์มหาวิทยาลัยเชียงใหม่
Copyright © by Chiang Mai University
All rights reserved

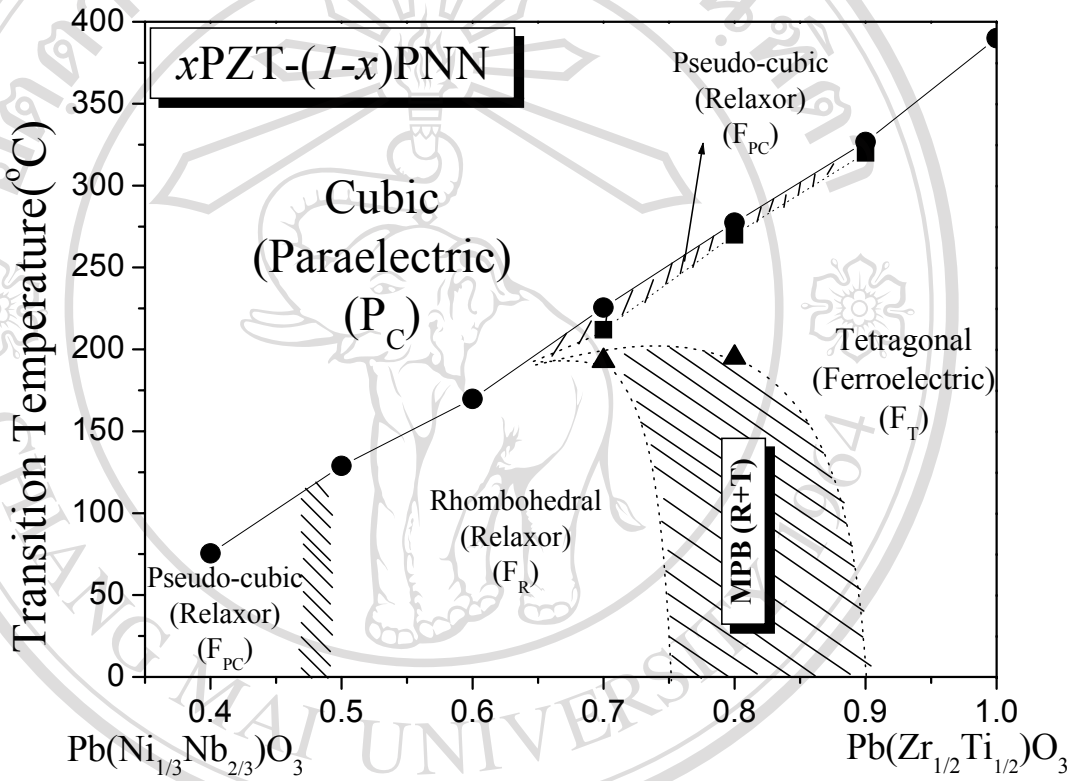

Figure 6.10 Phase diagram of *x*PZT – *(1-x)*PNN, *x = 0.4-0.9* binary system determined from room temperature XRD, Raman spectra and dielectric spectra as a function of temperature. The symbols refer to: ■ = the transition temperature fro ferroelectric (F_R, F_T and F_{PC})to relaxor (P_C); ● = the transition temperature from ferroelectric state (F_R, F_T and F_{PC}) paraelectric state (cubic); ▲ = the transition temperature from rhombohedral (F_R) to tetragonal(F_T)

ลิขสิทธิ์มหาวิทยาลัยเชียงใหม่
Copyright © by Chiang Mai University
All rights reserved